Nature of the $a_1(1420)$

M. Mikhasenko,[1] B. Ketzer,[1,*] and A. Sarantsev[1,2]

[1]*Universität Bonn, Helmholtz-Institut für Strahlen- und Kernphysik, 53115 Bonn, Germany*
[2]*NRC Kurchatov Institute, PNPI, 188300, Gatchina, Russia*

The resonancelike signal with axial-vector quantum numbers $J^{PC} = 1^{++}$ at a mass of 1420 MeV and a width of 140 MeV, recently observed by the COMPASS and VES experiments in the $f_0(980)\pi$ final state and tentatively called $a_1(1420)$, is discussed. Instead of a genuine new meson, we interpret this signal as a dynamical effect due to a singularity (branching point) in the triangle diagram formed by the processes $a_1(1260) \to K^\star \bar{K}$, $K^\star \to K\pi$, and $K\bar{K} \to f_0(980)$ (+c.c.). The amplitude for this diagram is calculated. The result exhibits a peak in the intensity with a sharp phase motion with respect to the dominant $a_1(1260) \to \rho\pi$ S-wave decay, in good agreement with the data. The branching ratio of $a_1(1260) \to f_0(980)\pi$ via the triangle diagram is estimated and compared to the dominant decay $a_1(1260) \to \rho\pi$.

I. INTRODUCTION

Understanding the quark interaction at low and intermediate energies is one of the most challenging tasks of the theory of strong interactions. To create a theoretical nonperturbative approach or, at least, to build a reliable model one should understand the nature of strongly interacting particles and their excitation spectrum. The classical quark model assumes that mesons are bound states of quarks and antiquarks, and groups the low-mass states into nonets with the same spin J, parity P, and charge-conjugation parity C, with fixed mass differences between nonet members. The second assumption is that the quark-antiquark interaction at large distances is governed by a linearly rising potential which explains the phenomenon of quark confinement and predicts the full spectrum of quark-antiquark excited states. The success of the quark model is indisputable: most of the known mesons correspond very well to the predicted scheme [1].

However, it seems that the meson spectrum is notably richer than that predicted by the quark model. There is a growing set of experimental observations of resonancelike structures in partial waves with quantum numbers which are forbidden for the quark-antiquark system or situated at masses which cannot be explained by the quark-antiquark model, see e.g. [2,3] and references therein.

Recently the COMPASS experiment [4–6] reported the observation of a small resonancelike signal with axial-vector quantum numbers $I^G(J^{PC}) = 1^-(1^{++})$ in the $f_0(980)\pi$ P-wave of the $\pi^-\pi^-\pi^+$ final state, produced by diffractive scattering of a 190 GeV π^- beam on a proton target. The signal was also confirmed by the VES experiment [7] in the $\pi^-\pi^0\pi^0$ final state. In both experiments, the three-pion final states were analyzed using a two-step partial-wave analysis technique. In the first step the data

were grouped in small bins of 3π-invariant mass and momentum transfer. The isobar model was employed to parametrize possible decays to three final pions. An isolated, relatively narrow peak was found in the intensity of the $1^-1^{++}f_0\pi P$-wave at a mass of around 1.4 GeV, accompanied by a sharp phase motion of this wave relative to other known resonances, with a phase variation exceeding 180°. In the second step of the COMPASS and VES analyses the spin-density matrix resulting from the first step was fitted with a model including Breit-Wigner resonances and background contributions. The new signal was described rather well with a hitherto unknown resonance, which was tentatively called $a_1(1420)$, with a mass $M_{a_1} \approx 1.42$ GeV and width $\Gamma_{a_1} \approx 0.14$ GeV. The interpretation of this signal as a new state in the framework of the quark model is difficult. It cannot be a radial excitation of $a_1(1260)$ which is expected to have a mass above 1650 MeV. It is also not expected that the radial excitation has a width which is much smaller than the one of the ground state. Therefore, this signal is to be considered either as a strong candidate for a four-quark bound state or a meson-meson molecular bound state or to be explained as a dynamical effect resulting from multiparticle interactions.

In the present paper we show that a signal of comparable strength, including the rapid phase motion, can be expected by the opening of the $K^\star \bar{K}$ decay channel for the isovector $a_1(1260)$, and the rescattering of the kaons. There are two isospin combinations of intermediate particles:

   (i) $a_1^-(1260) \to K^{\star 0}K^- \to \pi^- K^+ K^- \to \pi^- f_0$,
   (ii) $a_1^-(1260) \to K^{\star -}K^0 \to \pi^- \bar{K}^0 K^0 \to \pi^- f_0$.

The corresponding triangle diagram has a logarithmic singularity on the tail of the wide $a_1(1260)$ which is due to a very peculiar kinematic situation, in which all intermediate particles are almost on their mass shell, causing a resonancelike effect.

Recently, Wu *et al.* [8,9] showed that the same triangle singularity in the isospin-0 channel can account for the

*Bernhard.Ketzer@uni-bonn.de

anomalously large isospin violation effects observed by BESIII for $\eta(1407/1475)$ and $f_1(1420) \to f_0(980)\pi \to 3\pi$ [10]. A similar dynamic mechanism was suggested earlier by Achasow and Kozhevnikov [11] to explain the resonancelike signal observed in the $\phi\pi^0$ mass spectrum of the reaction $\pi^- p \to \phi\pi^0 n$ [12] by the decay of $\rho(1700) \to K^\star \bar{K}$ and the rescattering of $K\bar{K} \to \phi$. Triangle singularities are currently also being discussed in the context of the newly discovered XYZ quarkonium peaks [13].

Our paper is organized as follows. In Secs. II to IV, we only discuss the triangle diagram for process (i) with intermediate particles $(K^{\star 0}, K^+, K^-)$, the calculation for process (ii) proceeds analogously. In Sec. II the kinematic conditions for the appearance of the triangle singularity are analyzed. The amplitude for the triangle process is calculated in the following two sections. In Sec. III we first present an approach for calculating the imaginary part of the amplitude making use of Cutkosky cutting rules and the calculation of discontinuities. This method helps us to understand the structure of the amplitude singularities. In Sec. IV we then use an effective Lagrangian approach [14] to calculate the full amplitude, i.e. the real and imaginary parts, needed to predict the phase motion. In both sections, we start with the case of scalar particles to illustrate the underlying physics. In scalar theory the behavior of the amplitude is $\propto \log(s - s_0)$ near the singularity s_0. Since the amplitude behavior could be different in scalar theory and in interactions of particles with spin [11], then the realistic situation for particles with spin and finite width is calculated. We show that the singularity is removed only by including the finite width of unstable particles and gives a contribution $\sim \log \Gamma_{K^\star}$.

In Sec. V we estimate the branching ratio of $a_1(1260) \to f_0(980)\pi^-$, now including both isospin combinations, relative to its dominant decay channel $\rho\pi^-$, and compare the signal we expect for the triangle diagram to experimental values as reported in [6].

II. KINEMATIC CONDITIONS FOR TRIANGLE SINGULARITY

It is well known that logarithmic singularities arise in processes which proceed via the triangle diagram shown in Fig. 1. As was shown by a general analysis of singularities in scalar theory [15], the amplitude behavior near the branching point of a cut is $\propto \log(s - s_0)$, where s is an external invariant. The position of the singularity s_0 can be obtained from the simple conditions that all intermediate particles are on mass shell and are collinear to each other. It is given by the system of Lorentz-invariant Landau equations:

$$\begin{cases} k_i^2 = m_i^2, & i = 1\ldots3, \\ xk_{1\mu} - yk_{2\mu} + zk_{3\mu} = 0, & x, y, z \in [0,1], \quad (1) \\ x + y + z = 1, \end{cases}$$

with k_i and m_i the 4-momenta and masses of intermediate particles, respectively, and x, y, z the so-called Feynman parameters. The system of equations (1) for x, y, z is overdetermined, so it is solvable only in exceptional cases. For the special case of the decay of $a_1^-(1260)$ to $f_0(980)\pi^-$ through intermediate particles $(K^{\star-}, \bar{K}^0, K^0)$ or $(K^{\star 0}, K^+, K^-)$, and neglecting the finite width of the $f_0(980)$, the external momenta p_1 and p_2 depend only on $s = p_0^2$ (see Fig. 1 for the definition of p_i). Using kinematical relations between internal and external momenta it can be shown that the system (1) has solutions only if $\sqrt{s} = E_{1,2}$, where $E_1 = 1.42$ GeV, $E_2 = 1.46$ GeV. These pinch singularities are shown as dots in Fig. 2. As can be seen, the conditions $x, y, z \in [0, 1]$ are satisfied only for the first solution.

Here we give a simple kinematic explanation for the appearance of the singularity. The initial state $a_1(1260)$ with $J^{PC} = 1^{++}$ can decay to real $K^\star \bar{K} + $ c.c. starting from the threshold $\sqrt{s} = 1.39$ GeV. Then the $K^\star$ decays to real
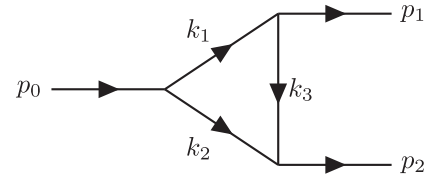

FIG. 1. The process $0 \to 1 + 2$ for particles with 4-momenta p_0, p_1, p_2, proceeding via a triangle diagram with intermediate particle momenta k_1, k_2, k_3.
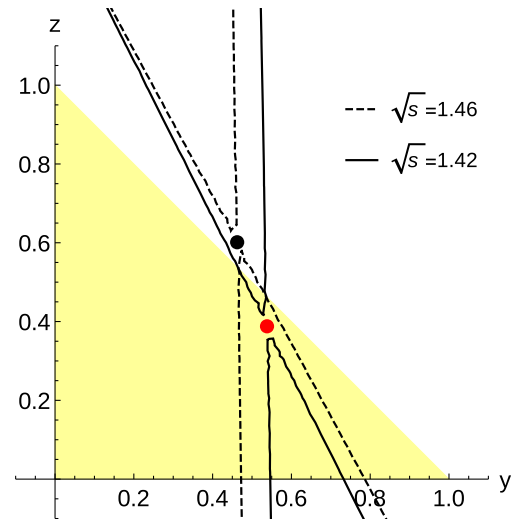

FIG. 2 (color online). Diagram illustrating the positions of singularities of the triangle diagram shown in Fig. 1 for the Feynman variables y, z. The shaded triangle is the kinematically allowed region. The dots are pinch singularities, corresponding to $\sqrt{s} = E_1$ (lower dot) and $\sqrt{s} = E_2$ (upper dot), respectively. The curves are solutions of $\Delta_{yz} + m_1^2(1 - y - z) = 0$ [see Eqs. (16) and (17)] for $\sqrt{s} = E_1$ (solid line) and $\sqrt{s} = E_2$ (dashed line).

K and π. Note that the K from $K^\star$ decay can go to the same direction as the $\bar{K}$, the ratio of velocities of $\bar{K}$ and K is a function of $\sqrt{s}$ as well as of the invariant mass of K and $\bar{K}$. The invariant mass of $\bar{K}K$ going in the same direction is equal to the mass of f_0 only if $\sqrt{s} = E_{1,2}$, but for E_2 the $\bar{K}$ is faster than the K and thus the K cannot catch up the $\bar{K}$ to form f_0. Only for the solution E_1 do the K and $\bar{K}$ proceed in the same direction with the K being faster than the $\bar{K}$.

The kinematics discussed here demonstrates a very peculiar situation in the decay of the $a_1(1260)$ to $K^\star \bar{K} + $ c.c: just above the two-body threshold, the rescattering in the triangle can happen with particles almost on mass shell.

III. IMAGINARY PART OF THE AMPLITUDE

In order to understand the structure of the amplitude, we first consider the imaginary part only, based on discontinuities. The technique was developed by Cutkosky [16], is described e.g. in the Gribov lectures [17], and was successfully applied by Achasov and Kozhevnikov for a similar process, $\rho' \to \phi\pi$ [11]. The imaginary part of the amplitude $\mathbb{M}$ of the diagram in Fig. 1 is related to the discontinuity across the cuts shown in Fig. 3 by

$$\text{Im}\mathbb{M}_{a_1 \to f_0 \pi} = \frac{1}{2}(\text{Disc}_{K^\star \bar{K}} + \text{Disc}_{K\bar{K}}). \qquad (2)$$

To calculate the discontinuities, we use the following expression:

$$\text{Disc} = \int \prod_{\text{cut}} \frac{d^3 k_i}{(2\pi)^3 2E_i^k} \times \left(\sum_{\text{polarization}} \mathbb{M}_1 \cdot \mathbb{M}_2^\star \right)$$
$$\times (2\pi)^4 \delta^4(\text{mom. cons.}), \qquad (3)$$

where $\mathbb{M}_{1,2}$ are matrix elements for processes on the left- and right-hand side of the cutting line, respectively (see Fig. 3). We are calling particles which are crossed by the cutting line cut particles. The integration is performed over all momentum space for cut particles, i.e. k_i are the momenta of cut particles, E_i^k are the corresponding energies. If a cut particle has spin we sum over all possible polarizations.
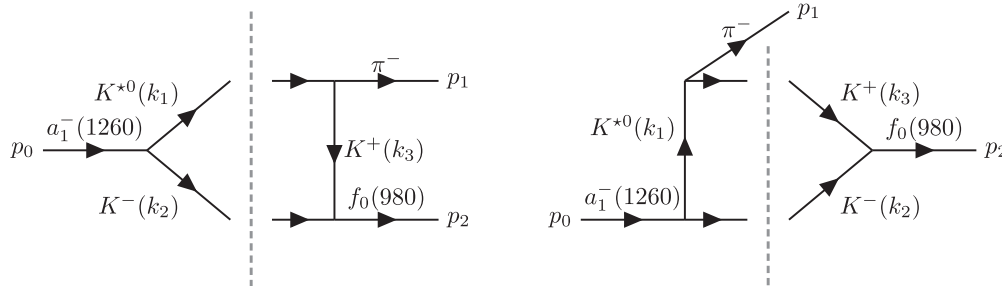
A. Simple model with scalar intermediate particles

For the case of scalar intermediate particles, the expressions for the discontinuities are

$$\text{Disc}_{K^\star \bar{K}}^{(\text{sc})} = g^3 \int \frac{d^3 k_1}{(2\pi)^3 2E_1^k} \frac{d^3 k_2}{(2\pi)^3 2E_2^k} \times \frac{1}{m_3^2 - k_3^2 + i\epsilon}$$
$$\times (2\pi)^4 \delta^4(p_0 - k_1 - k_2), \qquad (4)$$

$$\text{Disc}_{K\bar{K}}^{(\text{sc})} = g^3 \int \frac{d^3 k_2}{(2\pi)^3 2E_2^k} \frac{d^3 k_3}{(2\pi)^3 2E_3^k} \times \frac{1}{m_1^2 - k_1^2 - i\epsilon}$$
$$\times (2\pi)^4 \delta^4(k_3 + k_2 - p_2). \qquad (5)$$

Here, the products of matrix elements $\mathbb{M}_1 \cdot \mathbb{M}_2^\star$ are given by the coupling constants at the three vertices, which are set to g, and the propagator, which is a function of the angle between $\vec{k}_1$ and $\vec{p}_1$ in Eq. (4) and a function of the angle between $\vec{k}_2$ and $\vec{p}_1$ in Eq. (5). For both discontinuities, the cut particles ($K^\star$, K^- and K^+, K^-, respectively) are set on their mass shells. The integration with the delta function in Eq. (5) is performed in the f_0 rest frame. After carrying out the integration we arrive at the following expression:

$$\text{Im}\mathbb{M}_{a_1 \to f_0 \pi}^{(\text{sc})} = \frac{g^3}{16\pi} \left[\frac{1}{2|\vec{p}|\sqrt{s}} \log \frac{\tilde{A} + 1 + i\epsilon}{\tilde{A} - 1 + i\epsilon} \right.$$
$$\left. + \frac{1}{2|\vec{p}\,'||M_1} \log \frac{\tilde{C} + 1 - i\epsilon}{\tilde{C} - 1 - i\epsilon} \right], \qquad (6)$$

where the coefficients $\tilde{A}$, $\tilde{C}$ originate from the propagators,

$$\tilde{A} = (m_3^2 - m_1^2 - M_1^2 + 2E_1^p E_1^k)/(2|\vec{k}||\vec{p}|), \qquad (7)$$

$$\tilde{C} = (m_1^2 - s - m_2^2 + 2E_0' E_2^{k'})/(2|\vec{k}\,'||\vec{p}\,'|). \qquad (8)$$

Here, $M_i^2 = p_i^2$, $|\vec{k}| = \lambda^{1/2}(s, m_1^2, m_2^2)/(2\sqrt{s})$, $|\vec{p}| = \lambda^{1/2}(s, M_1^2, M_2^2)/(2\sqrt{s})$ are the momenta of the corresponding particles in the a_1 rest frame, with the Källen function

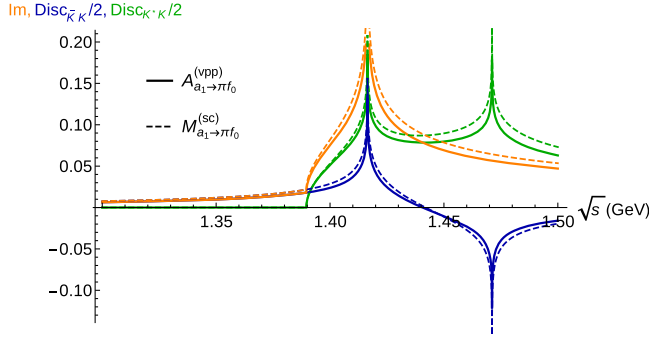$$\lambda(x, y, z) = x^2 + y^2 + z^2 - 2(xy + yz + zx), \qquad (9)$$

FIG. 3. Two possible cuts which contribute to the imaginary part of the matrix element of the process $a_1^-(1260) \to f_0(980)\pi^-$.

FIG. 4 (color online). Energy dependence of $\mathrm{Im}\mathbb{M}^{(sc)}_{a_1\to f_0\pi}(s)$ and $\mathrm{Im}\mathbb{A}^{(vpp)}_{a_1\to f_0\pi}(s)$ [dashed and full black (orange) lines, respectively]. The contributions of the discontinuities $K^\star\bar{K}$ and $K\bar{K}$ are shown by light gray (green) and dark gray (blue) lines, respectively.

and $E^k_1 = (s + m^2_1 - m^2_2)/(2\sqrt{s})$, $E^p_1 = (s + M^2_1 - M^2_2)/(2\sqrt{s})$. The primed variables are calculated in the f_0 rest frame: $|\vec{k}'| = \lambda^{1/2}(M^2_2, m^2_2, m^2_3)/(2M_2)$, $|\vec{p}'| = \lambda^{1/2}(s, M^2_1, M^2_2)/(2M_2)$ are the momenta of K^+ (K^-) and π^- (a^-_1). The corresponding expressions for the energy are $E^{k'}_2 = (M^2_2 + m^2_2 - m^2_3)/(2M_2)$, $E'_0 = (s + M^2_2 - M^2_1)/(2M_2)$. The imaginary parts of expressions (4) and (5) compensate for each other and consequently Eq. (6) is real.

The imaginary part of the amplitude $\mathrm{Im}\mathbb{M}^{(sc)}_{a_1\to f_0\pi}(s)$ as well as the contributions from the individual discontinuities are shown in Fig. 4 by dashed lines. One can clearly see the singularities at $\sqrt{s} = E_1$ and E_2. The singularity at E_2 is out of the kinematically allowed region of the reaction, so the sum of the two discontinuities is smooth at E_2. One can also notice that the imaginary part is not zero below the $K^\star\bar{K}$ threshold. Here, the contribution comes from $\mathrm{Disc}_{K\bar{K}}$, because the mass m_{f_0} is above the $2m_{K^\pm}$ threshold. Of

course, taking into account the real shape of $K^\star$ and f_0 will make the amplitude smoother, as shown in Sec. IV C, but the effect of the singularity at $\sqrt{s} = E_1$ will remain. This conclusion will also not change when the spin of the particles is taken into account, as will be shown in the next section.

B. Realistic case: intermediate particles with spin

In reality, the particles involved in the process carry quantum numbers different from the scalar particles used in the previous section. The $a_1(1260)$ with axial-vector quantum numbers $J^P = 1^+$ decays to $K^\star\bar{K}$ with vector (V) and pseudoscalar (P) quantum numbers, respectively. The $K^\star$ decays to two pseudoscalars, $K\pi$. We make use of the expressions for hadronic vertices given in Appendix A to take into account the spin structure of the particle involved.

The expressions for the discontinuities are then

$$\mathrm{Disc}^{(vpp)}_{K^\star\bar{K}} = g^3 \int \frac{d^3k_1}{(2\pi)^3 2E^k_1}\frac{d^3k_2}{(2\pi)^3 2E^k_2}$$
$$\times \frac{\varepsilon_{0\mu}(g^{\mu\nu} - \frac{k^\mu_1 k^\nu_1}{m^2_1})(p_1 - k_3)_\nu}{m^2_3 - k^2_3 + i\epsilon}$$
$$\times (2\pi)^4\delta^4(p_0 - k_1 - k_2), \qquad (10)$$

$$\mathrm{Disc}^{(vpp)}_{K\bar{K}} = g^3 \int \frac{d^3k_2}{(2\pi)^3 2E^k_2}\frac{d^3k_3}{(2\pi)^3 2E^k_3}$$
$$\times \frac{\varepsilon_{0\mu}(g^{\mu\nu} - \frac{k^\mu_1 k^\nu_1}{m^2_1})(p_1 - k_3)_\nu}{m^2_1 - k^2_1 - i\epsilon}$$
$$\times (2\pi)^4\delta^4(k_3 + k_2 - p_2). \qquad (11)$$

Here ε_0 is the polarization vector of the a_1; otherwise we use the notation shown in Fig. 3.
After integration, we have

$$\mathrm{Disc}^{(vpp)}_{K^\star\bar{K}} = g^3 \frac{1}{8\pi}\frac{2|\vec{k}|}{\sqrt{s}}(\varepsilon_0(p_1 - p_2)) \times \frac{M^2_1 + m^2_1 - m^2_3}{4m^2_1\vec{p}^2_1}\left[1 + \left(-\frac{|\vec{p}|}{|\vec{k}|}\frac{m^2_1}{M^2_1 + m^2_1 - m^2_3} + \frac{\tilde{A}}{2}\right)\log\frac{\tilde{A} - 1 + i\epsilon}{\tilde{A} + 1 + i\epsilon}\right], \qquad (12)$$

$$\mathrm{Disc}^{(vpp)}_{K\bar{K}} = -g^3 \frac{1}{8\pi}\frac{2|\vec{k}'|}{M_2}(\varepsilon_0(p_1 - p_2)) \times \frac{M^2_1 + m^2_1 - m^2_3}{4m^2_1\vec{p}'^2}\frac{E'_0}{M_2}$$
$$\times \left[1 + \left(\frac{|\vec{p}'|}{|\vec{k}'|}\frac{2m^2_1M_2 - (M^2_1 + m^2_1 - m^2_3)E^{k'}_2}{(M^2_1 + m^2_1 - m^2_3)E'_0} + \frac{\tilde{C}}{2}\right)\log\frac{\tilde{C} - 1 - i\epsilon}{\tilde{C} + 1 - i\epsilon}\right]. \qquad (13)$$

We use the same notation as in the previous section. The P-wave from $K^\star$ decay is propagated to the $f_0\pi$ P-wave. So we have a factor $[\varepsilon_0(p_1 - p_2)]$ in the final expression for the imaginary part of the matrix element. We separate it to compare the result with the scalar case:

$$\mathbb{M}_{a_1\to f_0\pi}^{(vpp)} = g^3 \mathbb{A}_{a_1\to f_0\pi}^{(vpp)}[\varepsilon_0(p_1 - p_2)]. \tag{14}$$

$\mathbb{A}_{a_1\to f_0\pi}^{(vpp)}$ is plotted in Fig. 4 together with the result from the scalar theory. The two results are obviously very similar.

IV. FULL AMPLITUDE FOR $a_1^-(1260) \to f_0(980)\pi^-$ VIA $K^{\star 0}K^+K^-$ TRIANGLE

After the calculation of the imaginary part of the amplitude based on discontinuities we proceed now to the calculation of the full amplitude for the triangle diagram shown in Fig. 5 using Feynman rules for hadronic processes in an effective Lagrangian approach [14] (see Appendix A for the parametrization of vertices). As in the previous section, we start from the simple case of scalar particles, and generalize to particles with spin in Sec. IV B.

A. Simple model with scalar intermediate particles

In case of vertices involving scalar particles only the matrix element for the triangle diagram in Fig. 5 is

$$\mathbb{M}_{a_1\to f_0\pi}^{(sc)} = g^3 \int \frac{d^4 k_1}{(2\pi)^4 i} \frac{1}{(m_1^2 - k_1^2 - i\epsilon)(m_2^2 - (p_0 - k_1)^2 - i\epsilon)(m_3^2 - (k_1 - p_1)^2 - i\epsilon)}, \tag{15}$$

We calculate the integral using the standard technique of Feynman parameters and Wick rotation, which is described in more detail in Appendix B 1:

$$\mathbb{M}_{a_1\to f_0\pi}^{(sc)} = \frac{g^3}{16\pi^2} \int_0^1 dy \int_0^{1-y} dz \frac{1}{\Delta_{yz} + m_1^2(1 - y - z) - i\epsilon}, \tag{16}$$

where Δ_{yz} is given by

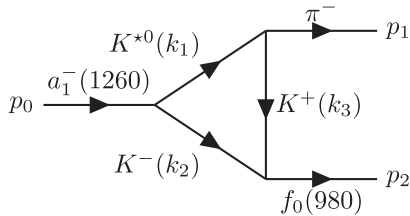$$\Delta_{yz} = ym_2^2 + zm_3^2 - y(1 - y - z)p_0^2 - z(1 - z - y)p_1^2 - yzp_2^2. \tag{17}$$

FIG. 5. $a_1(1320) \to f_0(980)\pi^-$ triangle diagram.

Equation (16) is evaluated numerically and the real and imaginary parts are shown in Fig. 6 (left panel). If the widths of all the intermediate particles are set to zero, the detailed structure of the amplitude becomes apparent. The imaginary part starts to grow rapidly from threshold $\sqrt{s_{th}} = m_K + m_{K^\star}$ and goes to infinity when $\sqrt{s} = E_1$. It exactly reproduces our result from Sec. III shown in Fig. 4. The real part has a cusp at the threshold, then sharply drops below zero at $\sqrt{s} = E_1$ and becomes stable for higher values of $\sqrt{s}$.
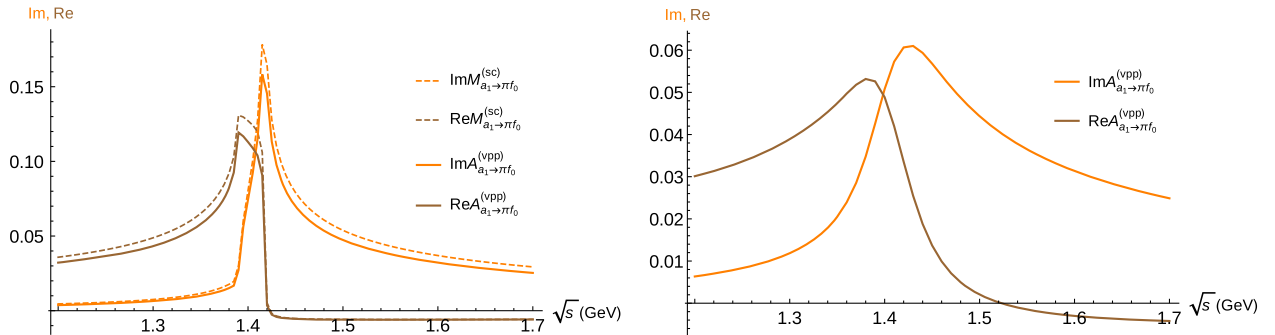
FIG. 6 (color online). (Left panel) Real [black (brown)] and imaginary [gray (orange)] parts of $\mathbb{A}_{a_1\to f_0\pi}^{(vpp)}(s)$ and $\mathbb{M}_{a_1\to f_0\pi}^{(sc)}(s)$, respectively. (Right panel) Real [black (brown)] and imaginary [gray (orange)] parts of $\mathbb{A}_{a_1\to f_0\pi}^{(vpp)}(s)$ when the finite width of $K^\star$ is taken into account in the VPP case.

B. Realistic case: intermediate particles with spin

For the realistic case of vector and pseudoscalar intermediate particles the expression for the matrix element is

$$\mathbb{M}^{(\text{vpp})}_{a_1 \to f_0 \pi} = g^3 \int \frac{\mathrm{d}k_1^4}{(2\pi)^4 i} \frac{\varepsilon_{0\mu}(g^{\mu\nu} - \frac{k_1^\mu k_1^\nu}{k_1^2})(p_1 - k_3)_\nu}{(m_1^2 - k_1^2 - i\epsilon)(m_2^2 - (p_0 - k_1)^2 - i\epsilon)(m_3^2 - (k_1 - p_1)^2 - i\epsilon)}. \tag{18}$$

We can apply the same procedure as in Sec. IV A, introducing Feynman parameters and performing a Wick rotation, and then calculate the resulting integral numerically. The details of the calculation are shown in Appendix B 2. Using the relation between $\mathbb{A}^{(\text{vpp})}_{a_1 \to f_0 \pi}$ and $\mathbb{M}^{(\text{vpp})}_{a_1 \to f_0 \pi}$ given in Eq. (14), the result is

$$\mathbb{A}^{(\text{vpp})}_{a_1 \to f_0 \pi} = \frac{1}{16\pi^2} \int_0^1 \mathrm{d}y \int_0^{1-y} \mathrm{d}z \frac{1}{\Delta_{yz} + m_1^2(1 - y - z) - i\epsilon}$$
$$+ \frac{1}{16\pi^2} \int_0^1 \mathrm{d}y \int_0^{1-y} \mathrm{d}z \int_0^{1-y-z} \mathrm{d}x \left[\frac{yz(p_0 \cdot p_1) + z^2 p_1^2}{(\Delta_{yz} + m_1^2 x - i\epsilon)^2} - \frac{1/4}{\Delta_{yz} + m_1^2 x - i\epsilon} \right]. \tag{19}$$

The real and imaginary parts of $\mathbb{A}^{(\text{vpp})}_{a_1 \to f_0 \pi}$ are compared to the scalar case in Fig. 6 (left panel). For both real and imaginary parts, the result for the VPP case is very similar to the scalar one, as was already shown for the imaginary part in Sec. III.

C. Corrections to $K^\star \to K\pi$ vertex

There are two additional corrections to be taken into account in order to arrive at a realistic estimate of the triangle amplitude:

(1) Finite widths of intermediate particles. Until now we have assumed that the particles in the loop are stable ($\epsilon \to 0$). While this is reasonable for K, the width of $K^\star$ is $\Gamma_{K^\star} = 0.05$ GeV,

(2) P-wave tail suppression. In the VPP case the $K^\star$ decays to $K\pi$ in a P-wave, which is propagated to the $f_0 \pi$ final state, $|\mathbb{M}^{(\text{vpp})}_{a_1 \to f_0 \pi}|^2 \sim (\mathbb{A}^{(\text{vpp})}_{a_1 \to f_0 \pi})^2 |\vec{p}_\pi|^2$ ($|\vec{p}_\pi|$ is $a_1 \to f_0 \pi$ break-up momentum). Therefore, the final f_0 and π effectively are in a P-wave. This gives rise to an enhanced, unphysical tail in the signal intensity.

To take into account the finite width of the intermediate particles we substitute the propagators of stable particles with resonance propagators. Technically this leads to substitutions $m_j^2 \to m_j^2 - im_j\Gamma_j$. Including such a term for the $K^\star$ propagator in Eq. (18) results in a smoother behavior of the amplitude, as shown in Fig. 6 (right panel). The singularity at $\sqrt{s} = E_1 = 1.42$ GeV is now limited and proportional to $\log \Gamma_{K^\star}$.

For a two-body decay with orbital angular momentum L, the amplitude behaves like p^L close to threshold due to the centrifugal barrier. Far away from threshold this is no longer correct because of the finiteness of the strong interaction. Accounting for the finiteness of interaction, however, is not unique. For a direct decay of a resonance

phenomenological form factors are usually used, which come from a classical potential model. These could be Blatt-Weisskopf barrier factors [18] or exponential factors for finite meson-size corrections [19]. Another phenomenological approach is to introduce a simple left-hand singularity in the amplitude as a vertex form factor [20]. We demonstrate here that the latter approach, where a pole is introduced in the amplitude to account for the $K^\star$ P-wave decay, gives a reasonable result. To do so, we include in Eq. (18) a factor

$$F(k_1) = \frac{C}{M^2 - k_1^2} \tag{20}$$

under the integral, where M is the position of the left-hand singularity and C is a constant normalized to the $K^\star \to K\pi$ decay from its mass shell, $C = M^2 - m_{K^\star}^2$. Above the $K\pi$ threshold this correction behaves like a D-wave Blatt-Weisskopf factor [$F_{\text{bw}}^{(D)}$]. So M corresponds to the size of $K^\star$:

$$F_{\text{bw}}^{(D)}(\vec{p})^{-1/2} \sim 1 + R^2 |\vec{p}|^2 \approx 1$$
$$+ R^2 \frac{(k_1^2 - (m_\pi + m_K)^2)(k_1^2 - (m_\pi - m_K)^2)}{4k_1^2}$$
$$\approx 1 + R^2 \frac{(k_1^2 - (m_\pi + m_K)^2)}{4}$$
$$= -\frac{R^2}{4}(M^2 - k_1^2),$$
$$M^2 = (m_\pi + m_K)^2 - \frac{4}{R^2}. \tag{21}$$

With this form of correction, our standard approach of Feynman parameters and Wick rotation can be used; the details of the calculation are again moved to Appendix B 3. The final expression is
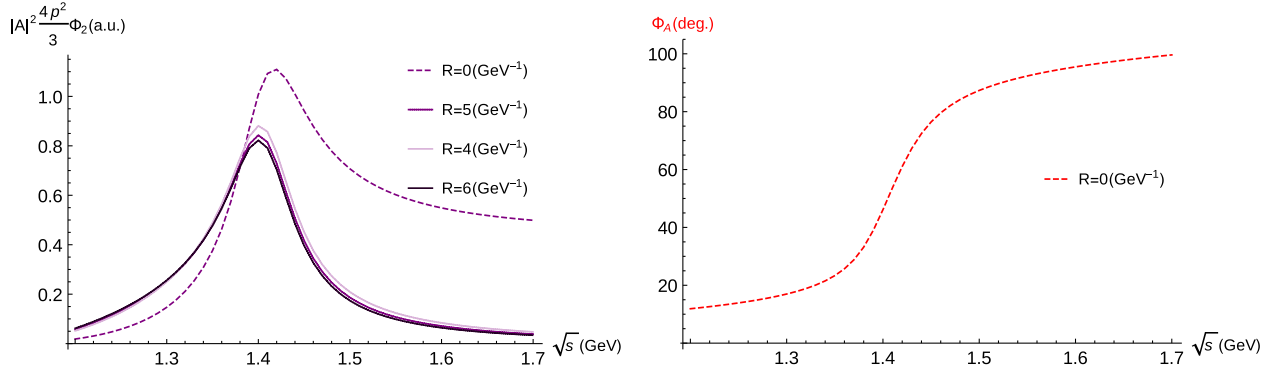
FIG. 7 (color online). The intensity (left panel) and the phase (right panel) of the final amplitude $\mathbb{A}_{a_1 \to f_0 \pi}(s)$ including the finite width of $K^\star$ and P-wave tail suppression [see Eq. (22)] as a function of $\sqrt{s}$ for different values of the suppression parameter R.

$$
\mathbb{A}_{a_1 \to f_0 \pi} = \frac{C}{16\pi^2} \int_0^1 dy \int_0^{1-y} dz \left\{ \frac{(1-y-z)}{(\Delta_{yz} + m_1^2(1-y-z))(\Delta_{yz} + M^2(1-y-z))} \right.
$$
$$
+ \frac{(z^2 p_1^2 + yz(p_1 \cdot p_2))(1-y-z)^2}{(\Delta_{yz} + m_1^2(1-y-z))(\Delta_{yz} + M^2(1-y-z))\Delta_{yz}}
$$
$$
\left. - \frac{1}{4}\frac{2}{M^2}\left[\frac{1}{m_1^2} \log \frac{\Delta_{yz} + m_1^2(1-y-z)}{\Delta_{yz}} - \frac{1}{m_1^2 - M^2} \log \frac{\Delta_{yz} + m_1^2(1-y-z)}{\Delta_{yz} + M^2(1-y-z)} \right] \right\}. \tag{22}
$$

This result including the finite width of $K^\star$ and the suppression of the P-wave tail at higher energies is plotted in Fig. 7. The left panel shows the intensity, $|\mathbb{A}_{a_1 \to f_0 \pi}|^2$ $(4p^2/3)\Phi_2$, where Φ_2 is the two-body phase space, for different values of the size parameter $R = 0.8$–1.2 fm, and also without suppression $(R = 0)$. The tail is indeed suppressed as expected, almost independent of the exact value of R. The phase of the signal for $R = 0$ (no suppression) is shown in the right panel. Including the suppression factor in the integral of Eq. (18) artificially shifts the phase to lower values with respect to the case with no suppression. The phase motion, i.e. the relative difference as a function of the energy, is not affected. Therefore we show only the phase for $R = 0$.

V. THE REACTION $\pi^- p \to a_1^-(1260)p \to f_0(980)\pi^- p$

A. Cross section

With a high-energy pion beam, as used in COMPASS and VES, the $a_1^-(1260)$ is produced in a diffractive process proceeding via t-channel Pomeron exchange between the beam π^- and the target proton, as shown in Fig. 8.

In order to estimate the intensity of the signal expected in the $f_0(980)\pi^-$ channel we calculate its intensity and phase difference compared to the dominant $a_1^-(1260) \to \rho^0 \pi^-$ decay, assuming that the signal in $f_0 \pi^-$ is entirely due to the triangle singularity in the decay $a_1^-(1260) \to f_0(980)\pi^-$. We denote the invariant mass squared of the a_1 by s, and the isobar invariant mass squared by s_{12} or s_{23}, respectively.

Factorizing out the production cross section $\sigma_{\text{prod}}(s)$ of the $a_1(1260)$, which is independent of the final state, the differential cross section for the full process $\pi^- p \to a_1^-(1260)p \to R\pi^- p \to \pi^- \pi^+ \pi^- p$ can be written as

$$
\frac{d\sigma}{ds} = \frac{\sigma_{\text{prod}}(s)}{4\pi} \left[\int \frac{ds_{12}}{2\pi} \frac{2m_{a_1}\Gamma_{a_1^- \to R\pi^-}(s, s_{12})}{(m_{a_1}^2 - s)^2 + m_{a_1}^2 \Gamma_{a_1}^2(s)} \right.
$$
$$
\times \frac{2m_R \Gamma_{R \to \pi^+ \pi^-}(s_{12})}{(m_R^2 - s_{12})^2 + m_R^2 \Gamma_R^2(s_{12})}
$$
$$
\left. + \{12 \leftrightarrow 23\} + \int d\Phi_{3\pi} \text{Interf}(s_{12}, s_{23}) \right], \tag{23}
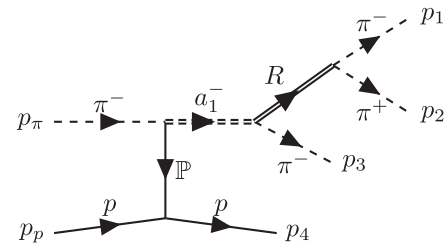$$

FIG. 8. Diagram for diffractive production of the $a_1(1260)$ by scattering of a high-energy π^- off a proton target, which remains intact. The $\pi^- \pi^+ \pi^-$ final state observed in the experiment is modeled by the decay of the a_1^- into a charged pion and a neutral isobar $R [\rho^0$ or $f_0(980)]$, which subsequently decays into two charged pions. The isobar can be formed either by $\pi_1^- \pi_2^+$ or by $\pi_2^+ \pi_3^-$.

where $\Gamma_{a \to bc}$ is the partial width for the two-body decay $a \to bc$, $m_{a_1,R}$ and $\Gamma_{a_1,R}$ are the pole masses and mass-dependent full widths of a_1 and R, respectively, and $d\Phi_{3\pi}$ is the 3π phase space. The first two terms constitute the contributions with the isobar in the $\pi_1^- \pi_2^+$ and in the $\pi_2^+ \pi_3^-$ subsystem, respectively. The third term is the

contribution of the interference between two processes. The latter is found to be very small for $a_1^- \to \rho^0 \pi^-$ (less than 2% for the a_1 decay from its mass shell) as well as for $a_1^- \to f_0 \pi^-$, so we will disregard that contribution and use the following equation for the cross section:

$$\frac{d\sigma}{ds} \approx \frac{\sigma_{\text{prod}}(s)}{2\pi} \int \frac{ds_{12}}{2\pi} \frac{2m_{a_1}\Gamma_{a_1^- \to R\pi^-}(s, s_{12})}{(m_{a_1}^2 - s)^2 + m_{a_1}^2 \Gamma_{a_1}^2(s)} \frac{2m_R \Gamma_{R \to \pi^+\pi^-}(s_{12})}{(m_R^2 - s_{12})^2 + m_R^2 \Gamma_R^2(s_{12})}. \tag{24}$$

The full widths of the $a_1(1260)$ and the isobars ρ^0, f_0 are described by Eq. (31) and Eqs. (28) and (35), respectively. The partial widths of the a_1 and the isobar decays are calculated by averaging the expressions for the square of the matrix elements of the corresponding hadronic vertices over the initial states and summing over the final ones and multiplying by the corresponding phase space. For the decay $a_1^-(1260) \to \rho^0 \pi^-$ (axial vector to vector and pseudoscalar, AVP), we have

$$\Gamma_{a_1^- \to \rho^0 \pi^-}(s, m^2) = \frac{1}{2m_{a_1}} g_{a_1^- \rho^0 \pi^-}^2 \left[1 + \frac{|\vec{p}_\rho|^2}{3m^2}\right] \times \frac{1}{8\pi} \frac{2|\vec{p}_\rho|}{\sqrt{s}}, \tag{25}$$

while for $a_1^-(1260) \to f_0 \pi^-$ (axial vector to pseudoscalar and scalar, APS), we get

$$\Gamma_{a_1^- \to f_0 \pi^-}(s, m^2) = \frac{1}{2m_{a_1}} g_{a_1^- f_0 \pi^-}^2(s, m^2) \frac{4|\vec{p}_{f_0}|^2}{3}$$
$$\times \frac{1}{8\pi} \frac{2|\vec{p}_{f_0}|}{\sqrt{s}}, \tag{26}$$

where $|\vec{p}_{\rho/f_0}(s, m^2)| = \lambda^{1/2}(s, m^2, m_\pi^2)/(2\sqrt{s})$ is the break-up momentum for the two-body decay of a particle with mass $\sqrt{s}$ to particles with masses $m = \sqrt{s_{12}}$ and m_π. The coupling of a_1^- to $f_0 \pi^-$ in Eq. (26) is given by

$$g_{a_1^- f_0 \pi^-}^2(s, m^2) = |\mathbb{A}_{a_1 \to f_0 \pi}|^2 (g_{a_1^- f_0 \pi^-}^{(K^\star \bar{K} + \text{c.c.})})^2, \tag{27}$$

where $\mathbb{A}_{a_1 \to f_0 \pi}$ is the triangle amplitude calculated in Eq. (22) and $g_{a_1^- f_0 \pi^-}^{(K^\star \bar{K} + \text{c.c.})}$ is an effective coupling which includes the couplings of the individual vertices in the triangle diagram, taking into account both isospin channels.

The expressions for the isobar decays are

$$\Gamma_{\rho^0 \to \pi^+\pi^-}(m^2) = \frac{1}{2m_\rho} g_{\rho^0 \pi^+\pi^-}^2 \frac{4|\vec{p}_\pi|^2}{3} \times \frac{1}{8\pi} \frac{2|\vec{p}_\pi|}{m}$$
$$\times \frac{1 + R_\rho^2 |\vec{p}_\pi(m_\rho^2)|^2}{1 + R_\rho^2 |\vec{p}_\pi(m^2)|^2}, \tag{28}$$

and

$$\Gamma_{f_0 \to \pi^+\pi^-}(m^2) = \frac{1}{2m_{f_0}} \frac{2}{3} g_{f_0\pi\pi}^2 \times \frac{1}{8\pi} \frac{2|\vec{p}_\pi|}{m} \approx \frac{2}{3} \bar{g}_{f_0\pi\pi} |\vec{p}_\pi|, \tag{29}$$

where the dimensionless coupling $\bar{g}_{f_0\pi\pi} = g_{f_0\pi\pi}^2/(8\pi m_{f_0}^2)$ has been introduced, and $|\vec{p}_\pi| = \lambda^{1/2}(m^2, m_\pi^2, m_\pi^2)/(2m)$ is the break-up momentum of the isobar with mass m to two pions. In Eq. (28) a Blatt-Weisskopf factor with $R_\rho = 5 \text{ GeV}^{-1}$ has been added to account for the P-wave decay of the ρ^0.

B. Evaluation of the couplings

To evaluate the magnitude of the $a_1 \to f_0\pi$ decay with respect to the $a_1 \to \rho\pi$ S-wave we take into account two possible isospin configurations of intermediate states $(K^{\star 0}K^-K^+)$ and $(K^{\star -}K^0\bar{K}^0)$ and evaluate the corresponding couplings. The table gives the couplings and Clebsch-Gordan coefficients for each vertex inside the loop of the two isospin configurations:

Vertex	$K^{\star 0}K^-K^+$	$K^{\star -}K^0\bar{K}^0$
$a_1^- K^\star \bar{K}$	$g_{a_1 K^\star \bar{K}}$	$g_{a_1 K^\star \bar{K}}$
$K^\star K\pi$	$\sqrt{2/3} g_{K^\star K\pi}$	$\sqrt{2/3} g_{K^\star K\pi}$
$f_0 K\bar{K}$	$\sqrt{1/2} g_{f_0 K\bar{K}}$	$\sqrt{1/2} g_{f_0 K\bar{K}}$

Since the isospin structure of both configurations is identical, the two diagrams add up. Disregarding the mass difference between charged and neutral kaons, the contributions of both are the same, so the effective coupling of process can be written as

$$g_{a_1^- f_0 \pi^-}^{(K^\star \bar{K} + \text{c.c.})} = \frac{2}{\sqrt{3}} g_{a_1 K^\star \bar{K}} g_{K^\star K\pi} g_{f_0 K\bar{K}}. \tag{30}$$

We first consider a_1 decays. The resonance is rather wide, so the energy dependence of the width should be taken into account. The best knowledge about a_1 decay channels and branching ratio comes from hadronic τ decay measurements [19,21,22]. For simplicity we consider only

the main contribution to the energy dependence of the width, which comes from the $a_1 \to \rho\pi$ S-wave,

$$\Gamma_{a_1}(s) = N \int_{4m_\pi^2}^{(\sqrt{s}-m_\pi)^2} \frac{ds_{12}}{2\pi} \frac{2|\vec{p}(s,s_{12})|}{\sqrt{s}}$$

$$\times \frac{2m_\rho \Gamma_{\rho^0 \to \pi^+\pi^-}(s_{12})}{(m_\rho^2 - s_{12})^2 + m_\rho^2 \Gamma_\rho^2(s_{12})}, \quad (31)$$

where $|\vec{p}(s,s_{12})| = \lambda^{1/2}(s,s_{12},m_\pi^2)/(2\sqrt{s})$, N is a normalization constant calculated from requiring $\Gamma_{a_1}(m_{a_1}^2) = 0.4$ GeV. We use the measured branching ratios, $\text{Br}(a_1 \to \rho\pi, S\text{-wave}) \approx 60\%$, $\text{Br}(a_1 \to K^\star \bar{K} + \text{c.c.}, S\text{-wave}) \approx 2.2\%$ to extract the ratio of the couplings. The ratio $g_{a_1\rho\pi}/g_{a_1K^\star\bar{K}}$ is calculated with the help of Eq. (24), where the energy dependence of the production mechanism is disregarded. For $a_1 \to \rho\pi$, a size correction form factor $\exp(-R^2|\vec{p}_\rho|^2)$, where $\vec{p}_\rho$ is the break-up momentum, is applied [19]. For $R > 0.5$ GeV^{-1}, the convergence of the integral over ds_{12} in Eq. (24) is achieved for an upper limit of the integration ≤ 5 GeV, while for $R = 0$ a higher limit is required. Varying R between 0 and 5 GeV^{-1}, and including the uncertainty due to the slow convergence for $R = 0$, the resulting ratio of the couplings is

$$\frac{g_{a_1\rho\pi}^2}{g_{a_1K^\star\bar{K}}^2} = \frac{2g_{a_1^-\rho^0\pi^-}^2}{g_{a_1^-K^{\star 0}K^-}^2 + g_{a_1^-K^{\star-}K^0}^2} \approx 6\text{--}10. \quad (32)$$

For the evaluation of the relative strength of the $f_0\pi$ signal in Sec. V C, we use $g_{a_1\rho\pi}^2/g_{a_1K^\star\bar{K}}^2 = 6$.

The width of $K^\star$ has been measured precisely and the branching to the $K\pi$ P-wave is 100% [1]. The corresponding coupling can thus be extracted from

$$\Gamma_{K^\star} = \frac{1}{2m_{K^\star}} g_{K^\star K\pi}^2 \frac{4|\vec{k}|^2}{3} \times \frac{1}{8\pi} \frac{2|\vec{k}|}{m_{K^\star}},$$

$$|\vec{k}| = \lambda^{1/2}(s, m_{K^\star}^2, m_\pi^2)/(2m_{K^\star}) \quad (33)$$

to be $g_{K^\star K\pi}^2 = 31.2$.

The parametrization of the f_0 is not trivial, since both decay channels ($f_0 \to 2\pi$, $f_0 \to 2K$) need to be taken into account. We make use of the Flatté parametrization [23] of the f_0 propagator and the decay width in Eq. (24),

$$\frac{2m_{f_0}\bar{g}_{f_0\pi\pi}|\vec{p}_\pi(s_{12})|}{|m_{f_0}^2 - s_{12} - im_{f_0}\Gamma_{f_0}(s_{12})|^2},$$

$$|\vec{p}_{\pi/K}(s_{12})| = \frac{1}{2}\sqrt{s_{12} - 4m_{\pi/K}^2}, \quad (34)$$

$$\Gamma_{f_0}(m^2) = \bar{g}_{f_0\pi\pi}|\vec{p}_\pi(m^2)| + \bar{g}_{f_0K\bar{K}}|\vec{p}_K(m^2)|. \quad (35)$$

The measurements of the branching ratio $\text{Br}(f_0 \to K\bar{K})/(\text{Br}(f_0 \to \pi\pi))$ and the ratio of couplings extracted therefrom, $R_{K/\pi} = g_{f_0K\bar{K}}^2/g_{f_0\pi\pi}^2 = \bar{g}_{f_0K\bar{K}}/\bar{g}_{f_0\pi\pi} \approx 4$, are rather consistent with each other [24,25]. The absolute values of the couplings, in contrast, are not known very well. For our estimation of the branching we use $g_{f_0\pi\pi} = 2.3$ GeV [26], so $\bar{g}_{f_0\pi\pi} = 0.21$, $\bar{g}_{f_0K\bar{K}} \approx 0.8$.

C. Evaluation of the branching ratio

The cross section calculated with the help of Eq. (24) for $a_1^-(1260) \to f_0\pi^- \to \pi^-\pi^+\pi^-$ is compared to the one for the dominant channel $a_1^-(1260) \to \rho^0\pi^- \to \pi^-\pi^+\pi^-$ in Fig. 9. Here, the peak of $a_1 \to \rho\pi$ has been normalized to 1, the $f_0\pi$ channel is shown in relative scale. Under the
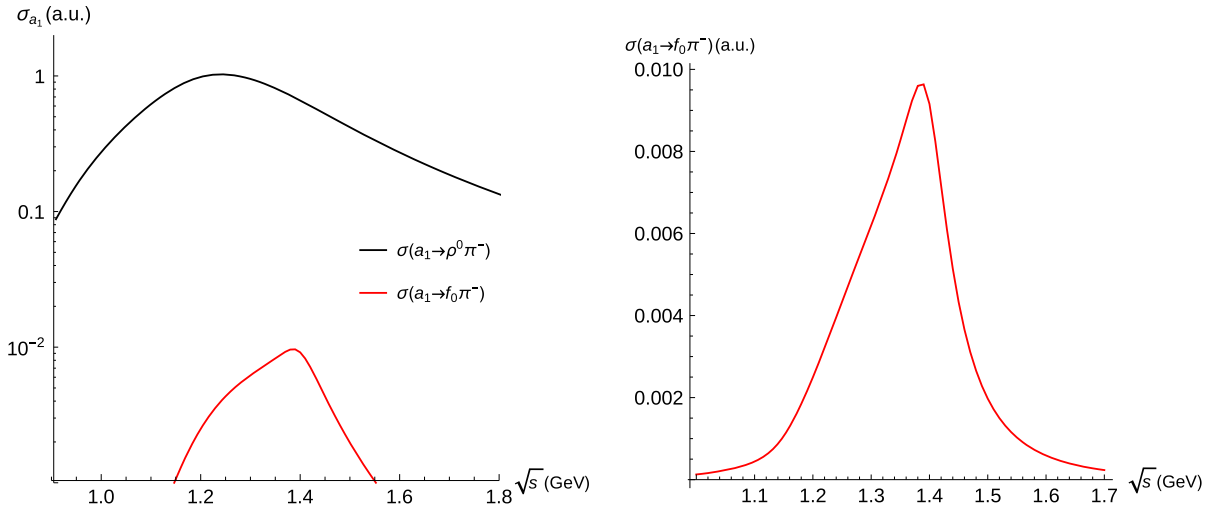

FIG. 9 (color online). Cross sections for the $a_1(1260)$ resonance as a function of invariant mass $\sqrt{s}$ in arbitrary units. (Left panel) Comparison of the dominant $a_1^- \to \rho^0\pi^-$ S-wave decay and the $a_1^- \to f_0\pi^-$ P-wave channel due to the rescattering of kaons. (Right panel) Pseudoresonant shape of $a_1^- \to f_0\pi^-$ in linear scale.

assumptions detailed in the previous subsection for the couplings, the peak-to-peak ratio is $\approx 1:100$, in very good agreement with the experimental result.

Finally, we discuss the reliability of our estimation and the factors which could affect the magnitude and the shape of the $f_0\pi$ peak. First of all, we assume that the decay of the $a_1(1260)$ resonance is the origin of $\rho\pi$ and $K^\star\bar{K} + \text{c.c.}$, which are rescattered to $f_0\pi$. In a hadron fixed-target experiment like COMPASS or VES, however, there may be other processes which contribute to the same final state, e.g. nonresonant Deck-like processes [27]. We expect a rather large contribution of the Deck-like background to the $\rho\pi$ S-wave signal [27] as well as to the $K^\star\bar{K}$ channel [28]. Taking into account these processes may cause the resulting ratio of the couplings to be different from Eq. (32).

Secondly, $\rho\pi \to f_0\pi$ rescattering plays an important role. Using the same method as in Sec. IV B one can show that the triangle diagram $a_1 \to \rho\pi \to f_0\pi$ gives a rather flat amplitude with a constant phase (magnitude $\approx 4\%$ of peak intensity of $K^\star\bar{K} + \text{c.c.} \to f_0\pi$). It interferes with the signal from $K^\star\bar{K} + \text{c.c.}$ and changes its intensity and phase. Taking into account this contribution is in principle possible, but requires the knowledge of the relative sign between $a_1 \to \rho\pi$ and $a_1 \to K^\star\bar{K}$, i.e. the relative sign of $s\bar{s}$ in a_1, which is unknown.

The third uncertainty comes from the shape of the f_0 and the corresponding coupling constants. We found that the shape of our signal is stable for different values of $g_{f_0\pi\pi}$ and $R_{K/\pi}$. The relative intensity, however, is proportional to $g_{f_0\pi\pi}^2 R_{K/\pi}$, which could therefore easily change by a factor of 2 depending on the input values.

VI. CONCLUSIONS

Even after many years of intense studies, both experimentally and theoretically, the excitation spectrum of hadrons is still not understood. This is especially true in the region of charm and bottom quarks, but also the light-quark sector sometimes bears surprises.

Present-day experiments are collecting extremely large event samples, with allow them to perform analyses with very small statistical uncertainties and permit them to find small signals which were not observable before. Recently, the COMPASS experiment has reported the observation of a resonancelike signal with axial-vector quantum numbers $J^{PC} = 1^{++}$ in a completely unexpected mass region only about 0.2 GeV above the ground state $a_1(1260)$, decaying to $f_0(980)\pi$.

In this paper we show that a resonancelike signal with a maximum intensity at 1.4 GeV, compatible with the experimental result, can be generated dynamically via a triangle singularity in the decay of the ground state $a_1(1260)$ to $K^\star\bar{K} + \text{c.c}$ and the subsequent rescattering of the K from $K^\star$ decay to form $f_0(980)$. This process also

generates a rather sharp phase motion, which is not locked to the phase of the wide $a_1(1260)$. The singularity appears in a kinematic region where the intermediate particles are collinear and on mass shell. The structure of the amplitude is investigated in two ways: first, the imaginary part is calculated using cutting rules; second, the full amplitude is evaluated using Feynman rules in order to obtain the imaginary and real parts. Both approaches are performed for the hypothetical case of scalar intermediate particles and for the realistic case of vector and pseudoscalar intermediate particles. It is shown that both cases give very similar results. For the final result of the triangle amplitude, we also include the finite width of the $K^\star$ and a phenomenological factor to suppress the tail due to the P-wave decay of the $K^\star$ at high energies. The inclusion of this factor, however, is not unique, and also spoils the beauty of the solution somewhat, because it artificially shifts the phase of the amplitude. In general, the treatment of decays with higher angular momenta inside loops in terms of analytical solutions certainly needs further investigations in the future.

We then estimate the magnitude of the signal expected in the $f_0(980)\pi$ channel due to the triangle singularity compared to the dominant decay of the $a_1(1260)$ to $\rho\pi$, also observed in the experiment. Our result gives a relative peak intensity of 1% for the $f_0\pi$ channel, with a rather large uncertainty which is due partly to poorly known couplings and partly to other rescattering processes like $a_1 \to \rho\pi \to f_0\pi$, which were neglected. The last process does not produce a singularity in the kinematically allowed region, but the corresponding amplitude interferes with the $K^\star\bar{K}$ amplitude and modifies its intensity and phase. In addition, we only consider the genuine $a_1(1260)$ resonance as a source for the triangle diagram, while it is known that in the reaction $\pi^- p \to 3\pi p$ there is a rather large contribution to the intensity in the $\rho\pi$ channel from nonresonant processes like the Deck effect, which may influence the relative branching ratio.
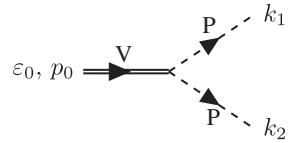
Despite these caveats, the dynamical interpretation of the $a_1(1420)$ presented in this paper captures the main effect and presumably accounts for a large fraction of the signal observed by COMPASS and VES. As a next step, one may fit our amplitude to the data and compare to the Breit-Wigner fit, and eventually extract better values for the coupling constants. The data sample on the a_1 from τ decays should also be large enough to observe the $f_0\pi$ peak if the data is fitted without phase locking of $f_0\pi$ with a_1. In general, the large data samples available nowadays both for light and heavy hadrons allow us to revisit effects which were already discussed more than 30 years ago, but were almost forgotten since then because data were too scarce to test them. These effects may now turn out to play an important role in our understanding of the hadron spectrum.
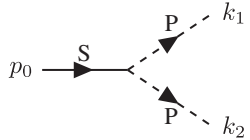
APPENDIX A: PARAMETRIZATION OF VERTICES AND FEYNMAN RULES

First we mention the approach we use to parametrize the vertices for interactions of particles. From symmetry considerations the Lorentz structure for the vertices is the following (we use S = scalar, P = pseudoscalar, V = vector, A = axial vector). For a vector → 2 pseudoscalar (VPP) vertex (P-wave) the structure is
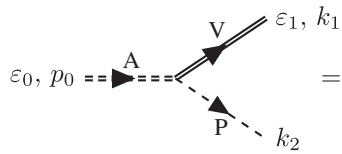

$$= g_{\text{VPP}} \; \varepsilon_\mu (k_1 - k_2)^\mu \qquad (A1)$$

for a scalar → 2 pseudoscalar (SPP) vertex (S-wave) it is

$$= g_{\text{SPP}} \qquad (A2)$$
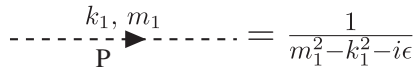
and for an axial vector → vector + pseudoscalar (AVP) vertex (S-wave) it is
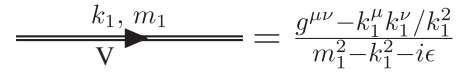
$$= g_{\text{AVP}} \; \varepsilon_0^\mu \varepsilon_{1\mu} \qquad (A3)$$

The propagator for a pseudoscalar particle is

$$= \frac{1}{m_1^2 - k_1^2 - i\epsilon} \qquad (A4)$$

while that for a vector particle is

$$= \frac{g^{\mu\nu} - k_1^\mu k_1^\nu / k_1^2}{m_1^2 - k_1^2 - i\epsilon} \qquad (A5)$$

APPENDIX B: CALCULATION OF INTEGRALS

In this section we calculate three integrals:

$$V_3 = \int \frac{\mathrm{d}k_1^4}{(2\pi)^4 i} \frac{1}{\Delta_1 \Delta_2 \Delta_3}, \qquad (B1)$$

$$V_4 = \int \frac{\mathrm{d}k_1^4}{(2\pi)^4 i} \frac{\varepsilon_{0\mu}(g^{\mu\nu} - \frac{k_1^\mu k_1^\nu}{k_1^2})(p_1 - k_3)_\nu}{\Delta_1 \Delta_2 \Delta_3}, \qquad (B2)$$

$$V_5 = \int \frac{\mathrm{d}k_1^4}{(2\pi)^4 i} \frac{\varepsilon_{0\mu}(g^{\mu\nu} - \frac{k_1^\mu k_1^\nu}{k_1^2})(p_1 - k_3)_\nu \times \frac{C}{M^2 - k_1^2}}{\Delta_1 \Delta_2 \Delta_3}, \qquad (B3)$$

where $\Delta_1 = m_1^2 - k_1^2 - i\epsilon$, $\Delta_2 = m_2^2 - (p_0 - k_1)^2 - i\epsilon$, $\Delta_3 = m_3^2 - (k_1 - p_1)^2 - i\epsilon$.

1. First integral

For the calculation of V_3, Feynman parameters (x, y, z) are introduced to rewrite the integral:

$$V_3 = \int_0^1 \int_0^1 \int_0^1 \mathrm{d}x\mathrm{d}y\mathrm{d}z 2!\delta(x + y + z - 1) \int \frac{\mathrm{d}^4 k}{(2\pi)^4 i} \frac{1}{D^3}, \qquad (B4)$$

where $D = x(m_1^2 - k_1^2 - i\epsilon) + y(m_2^2 - (p_0 - k_1)^2 - i\epsilon) + z(m_3^2 - (k_1 - p_1)^2 - i\epsilon)$. The quadratic form $D(k_1)$ can be reduced to diagonal form collecting terms with k_1 and extracting the full square. The condition $x + y + z = 1$ is used.

$$D = -(k_1 - yp_0 - zp_1)^2 + \Delta - i\epsilon, \qquad (B5)$$

$$\Delta = xm_1^2 + \Delta_{yz},$$

$$\Delta_{yz} = ym_2^2 + zm_3^2 - y(1 - y - z)p_0^2$$
$$- z(1 - z - y)p_1^2 - yzp_2^2. \qquad (B6)$$

After shifting the variable of integration $k_1 \rightarrow l = k_1 - yp_0 - zp_1$ we have

$$V_3 = \int_0^1 \int_0^1 \int_0^1 \mathrm{d}x\mathrm{d}y\mathrm{d}z 2!\delta(x + y + z - 1)$$
$$\times \int \frac{\mathrm{d}^4 l}{(2\pi)^4 i} \frac{1}{(-l^2 + \Delta - i\epsilon)^3}. \qquad (B7)$$

For the integration over l_0, notice that the denominator has poles when $l_0^2 = \vec{l}^2 + \Delta^2 - i\epsilon$. The positions of the poles are functions of the external invariants p_0^2, p_1^2, p_2^2 and the Feynman parameters. The basic idea which we use

is aimed at calculating the integral in the region where $p_0^2 < 0$, $p_1^2 < 0$, $p_2^2 < 0$, i.e. $\Delta > 0$ for all values of x, y, z. In that region we can rotate the contour of integration over l_0 counterclockwise (the Wick rotation) and integrate along the imaginary axis. We make use of the transfer of the integration variable l to Euler space with the integration variable l_E $(l^2 = -l_E^2)$, where the integration is much simpler. One has

$$V_3 = \int_0^1 \int_0^1 \int_0^1 \mathrm{d}x\mathrm{d}y\mathrm{d}z 2! \delta(x + y + z - 1)$$
$$\times \int \frac{\mathrm{d}^4 l_E}{(2\pi)^4} \frac{1}{(l_E^2 + \Delta - i\epsilon)^3}. \qquad \text{(B8)}$$

The next step is integration over l_E. As a result we have

$$V_3 = \frac{1}{16\pi^2} \int_0^1 \mathrm{d}y \int_0^{1-y} \mathrm{d}z \frac{1}{\Delta_{yz} + m_1^2(1 - y - z) - i\epsilon}. \qquad \text{(B9)}$$

Equation (B9) is simple enough for numerical integration.

2. Second integral

Let us consider integral V_4, Eq. (B2). The numerator can be simplified as

$$\varepsilon_{0\mu}\left(g^{\mu\nu} - \frac{k_1^\mu k_1^\nu}{k_1^2}\right)(p_1 - k_3)_\nu$$
$$= \varepsilon_{0\mu}\left(g^{\mu\nu} - \frac{k_1^\mu k_1^\nu}{k_1^2}\right)(2p_1 - k_1)_\nu$$
$$= 2(\varepsilon_0 \cdot p_1) + 2\frac{(\varepsilon_0 \cdot k_1)(k_1 \cdot p_1)}{-k_1^2}. \qquad \text{(B10)}$$

One can notice that k_1^2 in the numerator has the same form as $\Delta_0 = m_0^2 - k_1^2$ with mass $m_0^2 = 0$. The integral in Eq. (B2) is equal to

$$\frac{1}{2}V_4 = (\varepsilon_0 \cdot p_1)\int \frac{\mathrm{d}^4 k_1}{(2\pi)^4 i}\frac{1}{\Delta_1\Delta_2\Delta_3}$$
$$+ \int \frac{\mathrm{d}^4 k_1}{(2\pi)^4 i}\frac{(\varepsilon_0 \cdot k_1)(k_1 \cdot p_1)}{\Delta_0\Delta_1\Delta_2\Delta_3}. \qquad \text{(B11)}$$

The first integral in Eq. (B11) is equal to Eq. (B9). For the second one we introduce four Feynman parameters:

$$\int \frac{\mathrm{d}^4 k_1}{(2\pi)^4 i}\frac{(\varepsilon_0 \cdot k_1)(k_1 \cdot p_1)}{\Delta_0\Delta_1\Delta_2\Delta_3}$$
$$= \int_0^1 \mathrm{d}t \int_0^1 \mathrm{d}x \int_0^1 \mathrm{d}y \int_0^1 \mathrm{d}z 3! \delta(t + x + y + z - 1)$$
$$\times \int \frac{\mathrm{d}^4 k_1}{(2\pi)^4 i}\frac{(\varepsilon_0 \cdot k_1)(k_1 \cdot p_1)}{D_4^4}, \qquad \text{(B12)}$$

where for D_4 with the condition $x_0 + x_1 + x_2 + x_3 = 1$ we have the same expression as Eq. (B5). So the same shift of the integration variable k_1 is used, i.e. $k_1 \rightarrow l = k_1 - yp_0 - zp_1$.

The expression in the numerator can be written as

$$(\varepsilon_0 \cdot k_1)(k_1 \cdot p_1)$$
$$= l_\mu l_\nu \cdot [\varepsilon_0^\mu p_1^\nu] + l_\mu$$
$$\cdot [(zp_1^2 + y(p_1 \cdot p_2))\varepsilon_0^\mu + z(\varepsilon_0 \cdot p_1)p_1^\mu]$$
$$+ z(\varepsilon_0 \cdot p_1)(zp_1^2 + y(p_1 \cdot p_2)). \qquad \text{(B13)}$$

After Wick rotation and the integration over angular variables $\mathrm{d}\Omega_4$, the term proportional to l_μ gives zero and $l_\mu l_\nu \rightarrow -g_{\mu\nu} l_E^2/4$. So one arrives at

$$\int \frac{\mathrm{d}^4 k_1}{(2\pi)^4 i}\frac{(\varepsilon_0 \cdot k_1)(k_1 \cdot p_1)}{\Delta_0\Delta_1\Delta_2\Delta_3}$$
$$= \int_0^1 \mathrm{d}t \int_0^1 \mathrm{d}x \int_0^1 \mathrm{d}y \int_0^1 \mathrm{d}z 3! \delta(t + x + y + z - 1)$$
$$\times (\varepsilon_0 \cdot p_1)\left[-\frac{1}{4}\int \frac{\mathrm{d}^4 l_E}{(2\pi)^4}\frac{l_E^2}{(l_E^2 + \Delta - i\epsilon)^4}\right.$$
$$\left. + z(zp_1^2 + y(p_1 \cdot p_2))\int \frac{\mathrm{d}^4 l_E}{(2\pi)^4}\frac{1}{(l_E^2 + \Delta - i\epsilon)^4}\right]. \qquad \text{(B14)}$$

All integrals converge. The integration over $\mathrm{d}t$ is removed by a delta function:

$$\frac{1}{2}V_4 = \frac{(\varepsilon_0 \cdot p_1)}{16\pi^2}$$
$$\times \left\{\int_0^1 \mathrm{d}y \int_0^{1-y} \mathrm{d}z \frac{1}{\Delta_{yz} + m_1^2(1 - y - z) - i\epsilon}\right.$$
$$+ \int_0^1 \mathrm{d}y \int_0^{1-y} \mathrm{d}z \int_0^{1-y-z} \mathrm{d}x \left[\frac{yz(p_0 \cdot p_1) + z^2 p_1^2}{(\Delta_{yz} + m_1^2 x - i\epsilon)^2}\right.$$
$$\left.\left. - \frac{1/4}{\Delta_{yz} + m_1^2 x - i\epsilon}\right]\right\}, \qquad \text{(B15)}$$

with Δ_{yz} given by Eq. (B6).

3. Third integral

The calculation of V_5, Eq. (B3) proceeds similarly to V_4. The difference is that we have four poles instead of three in the denominator of Eq. (B3). First, one can simplify the numerator as in Eq. (B10):

$$\frac{1}{2C}V_5 = (\varepsilon_0 \cdot p_1) \int \frac{\mathrm{d}^4 k_1}{(2\pi)^4 i} \frac{1}{\Delta_1 \Delta_2 \Delta_3 \Delta_4}$$
$$+ \int \frac{\mathrm{d}^4 k_1}{(2\pi)^4 i} \frac{(\varepsilon_0 \cdot k_1)(k_1 \cdot p_1)}{\Delta_0 \Delta_1 \Delta_2 \Delta_3 \Delta_4}, \qquad \text{(B16)}$$

where $\Delta_4 = M^2 - k_1^2$.

We introduce four and five Feynman parameters for the integrals, respectively. The expression for the denominators are D_5^4 and $D_5'^5$:

$$D_5 = x(m_1^2 - k_1^2) + y(m_2^2 - (p_0 - k_1)^2)$$
$$+ z(m_3^2 - (k_1 - p_1)^2) + u(M^2 - k_1^2), \qquad \text{(B17)}$$

$$D_5' = t(-k_1^2) + x(m_1^2 - k_1^2) + y(m_2^2 - (p_0 - k_1)^2)$$
$$+ z(m_3^2 - (k_1 - p_1)^2) + u(M^2 - k_1^2). \qquad \text{(B18)}$$

Then we perform the same calculation as in Sec. B 2, and the result is

$$\frac{1}{2C}V_5 = \frac{(\varepsilon_0 \cdot p_1)}{16\pi^2} \int_0^1 \mathrm{d}y \int_0^{1-y} \mathrm{d}z \int_0^{1-y-z} \mathrm{d}x \left\{ \frac{1}{(\Delta_{yz} + m_1^2 x + M^2(1 - x - y - z) - i\epsilon)^2} \right.$$
$$\left. + \int_0^{1-x-y-z} \mathrm{d}u \left[\frac{yz(p_0 \cdot p_1) + z^2 p_1^2}{(\Delta_{yz} + m_1^2 x + M^2 u - i\epsilon)^3} - \frac{1/4}{(\Delta_{yz} + m_1^2 x + M^2 u - i\epsilon)^2} \right] \right\}, \qquad \text{(B19)}$$

where Δ_{yz} is given by Eq. (B6). To make the expression simpler and convenient for a numerical evaluation, we carry out the integration over $\mathrm{d}x$ and $\mathrm{d}y$ explicitly:

$$\frac{1}{2C}V_5 = \frac{1}{16\pi^2} \int_0^1 \mathrm{d}y \int_0^{1-y} \mathrm{d}z \left\{ \frac{(1 - y - z)}{(\Delta_{yz} + m_1^2(1 - y - z) - i\epsilon)(\Delta_{yz} + M^2(1 - y - z) - i\epsilon)} \right.$$
$$+ \frac{(z^2 p_1^2 + yz(p_1 \cdot p_2))(1 - y - z)^2}{(\Delta_{yz} + m_1^2(1 - y - z) - i\epsilon)(\Delta_{yz} + M^2(1 - y - z) - i\epsilon)(\Delta_{yz} - i\epsilon)}$$
$$\left. - \frac{1}{4}\frac{2}{M^2} \left[\frac{1}{m_1^2} \log \frac{\Delta_{yz} + m_1^2(1 - y - z) - i\epsilon}{\Delta_{yz} - i\epsilon} - \frac{1}{m_1^2 - M^2} \log \frac{\Delta_{yz} + m_1^2(1 - y - z) - i\epsilon}{\Delta_{yz} + M^2(1 - y - z) - i\epsilon} \right] \right\}. \qquad \text{(B20)}$$

[1] K. A. Olive *et al.* (Particle Data Group), Review of Particle Physics, Chin. Phys. C **38**, 090001 (2014).

[2] E. Klempt and A. Zaitsev, Glueballs, hybrids, multiquarks: Experimental facts versus QCD inspired concepts, Phys. Rep. **454**, 1 (2007).

[3] N. Brambilla *et al.*, QCD and strongly coupled gauge theories: challenges and perspectives, Eur. Phys. J. C **74**, 2981 (2014).

[4] C. Adolph *et al.* (COMPASS Collaboration), Observation of a new narrow axial-vector meson $a_1(1420)$, arXiv: 1501.05732 (to be published).

[5] S. Paul (COMPASS Collaboration), Precision spectroscopy with COMPASS and the observation of a new iso-vector resonance, EPJ Web Conf. **73**, 03002 (2014).

[6] B. Ketzer (COMPASS Collaboration), Precision studies of light mesons at COMPASS, *Proc. Sci.*, Hadron2013 (2014) 011 [arXiv:1403.4884].

[7] Y. Khokhlov *et al.* (VES Collaboration), Partial wave analyses of the $\pi^- \pi^0 \pi^0$ and $\pi^- \pi^0$ systems with VES setup, *Proc. Sci.*, Hadron2013 (2014) 088.

[8] J.-J. Wu, X.-H. Liu, Q. Zhao, and B.-S. Zou, Puzzle of Anomalously Large Isospin Violations in $\eta(1405/1475) \to 3\pi$, Phys. Rev. Lett. **108**, 081803 (2012).

[9] X.-G. Wu, J.-J. Wu, Q. Zhao, and B.-S. Zou, Understanding the property of $\eta(1405/1475)$ in the J/ψ radiative decay, Phys. Rev. D **87**, 014023 (2013).

[10] M. Ablikim *et al.* (BESIII Collaboration), First Observation of $\eta(1405)$ Decays into $f_0(980)\pi^0$, Phys. Rev. Lett. **108**, 182001 (2012).

[11] N. N. Achasov and A. A. Kozhevnikov, On the nature of $C(1480)$ resonance, Z. Phys. C **48**, 121 (1990).

[12] S. Bityukov *et al.*, Study of a possible exotic 1.5 GeV meson decaying into $\phi\pi^0$, Phys. Lett. B **188**, 383 (1987).

[13] A. P. Szczepaniak, Triangle singularities and XYZ quarkonium peaks, arXiv:1501.01691.

[14] U.-G. Meissner, Low-energy hadron physics from effective chiral Lagrangians with vector mesons, Phys. Rep. **161**, 213 (1988).

[15] L. D. Landau, On analytic properties of vertex parts in quantum field theory, Nucl. Phys. **13**, 181 (1959).

[16] R. E. Cutkosky, Singularities and Discontinuities of Feynman Amplitudes, J. Math. Phys. (N.Y.) **1**, 429 (1960).

[17] V. N. Gribov, Y. L. Dokshitzer, and J. Nyiri, Strong Interactions of Hadrons at High Energies: Gribov Lectures on Theoretical Physics, *Cambridge Monographs on Particle Physics, Nuclear Physics and Cosmology* Vol. 27 (Cambridge University Press, Cambridge, England, 2009).

[18] J. M. Blatt and V. F. Weisskopf, *Theoretical Nuclear Physics* (Wiley, New York, 1952).

[19] D. M. Asner *et al.* (CLEO Collaboration), Hadronic structure in the decay $\tau^- \to \nu_\tau \pi^- \pi^0 \pi^0$ and the sign of the tau neutrino helicity, Phys. Rev. D **61**, 012002 (1999).

[20] V. Anisovich, A. Kondashov, Y. Prokoshkin, S. Sadovsky, and A. Sarantsev, Two-pion spectra for the reaction $\pi^- p \to \pi^0 \pi^0 n$ at a pion momentum of 38 GeV/c and combined analysis of GAMS, Crystal Barrel, and BNL data, Phys. At. Nucl. **63**, 1410 (2000).

[21] R. A. Briere *et al.* (CLEO Collaboration), Branching Fractions of τ Leptons to Three Charged Hadrons, Phys. Rev. Lett. **90**, 181802 (2003).

[22] T. E. Coan *et al.* (CLEO Collaboration), Wess-Zumino Current and the Structure of the Decay $\tau^- \to K^- \pi^- K^+ \nu_\tau$, Phys. Rev. Lett. **92**, 232001 (2004).

[23] S. M. Flatté, Coupled-channel analysis of the $\pi\eta$ and $K\bar{K}$ systems near $K\bar{K}$ threshold, Phys. Lett. **63B**, 224 (1976).

[24] V. Baru, J. Haidenbauer, C. Hanhart, A. E. Kudryavtsev, and U.-G. Meissner, Flatté-like distributions and the $a_0(980)/f_0(980)$ mesons, Eur. Phys. J. A **23**, 523 (2005).

[25] M. Ablikim *et al.* (BES Collaboration), Resonances in $J/\Psi \to \phi\pi^+\pi^-$ and $\phi K^+ K^-$, Phys. Lett. B **607**, 243 (2005).

[26] R. García-Martín, R. Kamiński, J. R. Peláez, and J. Ruiz de Elvira, Precise Determination of the $f_0(600)$ and $f_0(980)$ Pole Parameters from a Dispersive Data Analysis, Phys. Rev. Lett. **107**, 072001 (2011).

[27] G. Ascoli, R. Cutler, L. M. Jones, U. Kruse, T. Roberts, B. Weinstein, and H. W. Wyld, Deck-model calculation of $\pi^- p \to \pi^- \pi^+ \pi^- p$, Phys. Rev. D **9**, 1963 (1974).

[28] E. B. Berdnikov *et al.* (VES Collaboration), Study of the reaction $\pi^- A \to K^+ K^- \pi^- A$ at 37 GeV/c, Phys. Lett. B **337**, 219 (1994).